Electronic Supplementary Information for Dalton Transactions
This journal is © The Royal Society of Chemistry 2007

Supporting information

Organic-Inorganic Hybrid Materials Constructed from Inorganic Lanthanide Sulfate Skeletons and Organic 4, 5-imidazoledicarboxylic acid

Yan-Qiong Sun,[a] and Guo-Yu Yang*[,a,b]

[a]State Key Laboratory of Structural Chemistry, Fujian Institute of Research on the Structure of Matter, Chinese Academy of Sciences, Fuzhou, Fujian 350002, China; [b] State Key Laboratory of Rare Earth Materials Chemistry and Applications, Peking University, Beijing 100871, China

This journal is © The Royal Society of Chemistry 2007

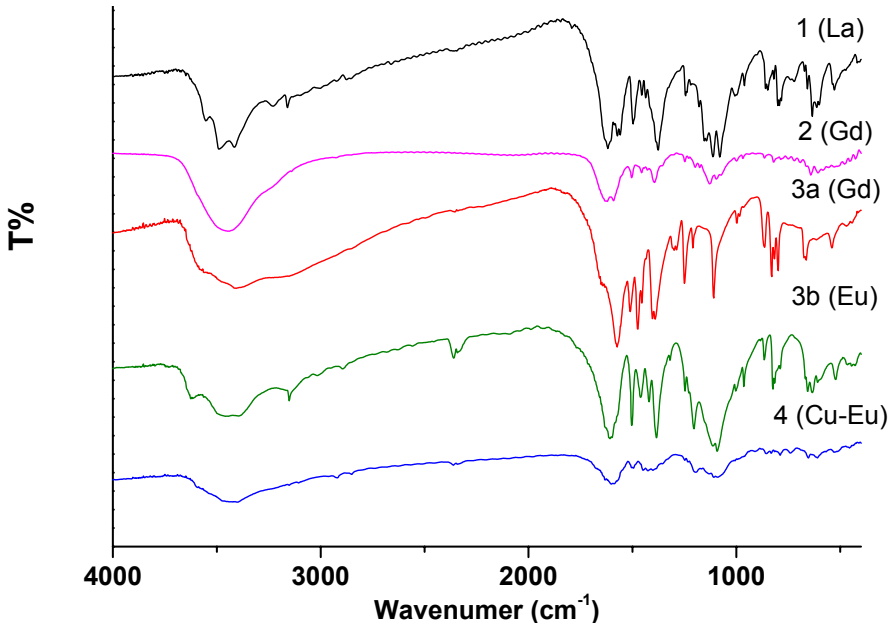

(a)

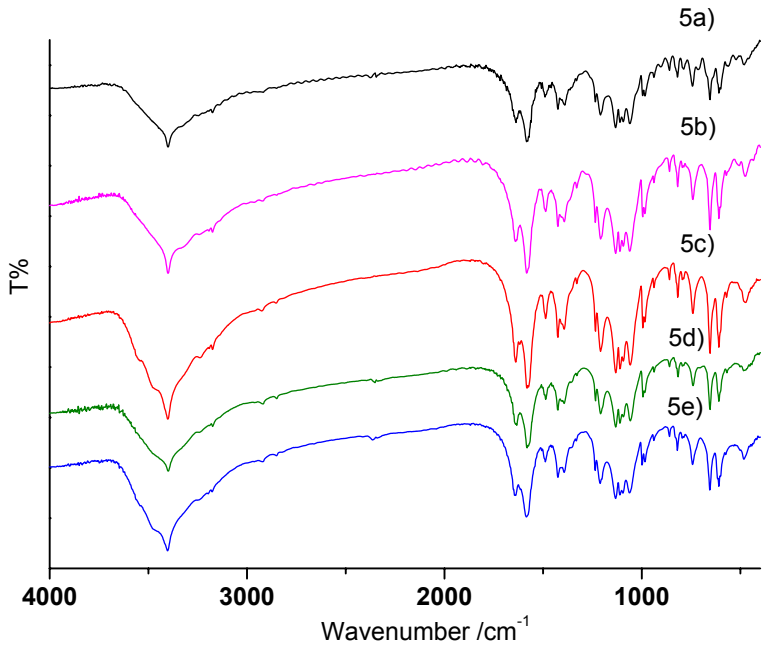

(b)

Figure S1. (a) IR spectra of $La_2(SO_4)(Himdc)_2(H_2O)_2$ (**1**), $[Gd_2(SO_4)_2(Himdc)(H_2O)_3]\cdot H_2O$ (**2**), $[Ln_2(SO_4)_2(Himdc)_2(H_2O)_3]\cdot H_2O$ (Ln = Gd **3a**, Eu **3b**) , $[Eu_6Cu(SO_4)_6(Himdc)_4(H_2O)_{14}]$ (**4**). (b) IR spectra of [Ln(Himc)$(SO_4)(H_2O)$] (Ln = Eu **5a**, Dy **5b**, Tb **5c**, Gd **5d**, Er **5e**).

In Figure S1a, the peak around 3400 cm^{-1} corresponds to the stretching bands of N-H, indicating that the ligand have been deprotonated to generate $Himdc^{2-}$. The peaks around 1600 cm^{-1} correspond to the stretching bands of C=O. The strong broad bands at 1104cm^{-1} can be assigned to the stretching vibrations of SO_4^{2-}. In Figure S1b, the sharp peak at 3400 cm^{-1} corresponds to the stretching bands of N-H, indicating that the H_2imc ligand have been deprotonated to

generate Himc ligand. The peaks at 1637 and 1582 cm^{-1} correspond to the stretching bands of C=O. The strong bands at the region of 1132-1052 cm^{-1} can be assigned to the stretching vibrations of SO_4^{2-} group.

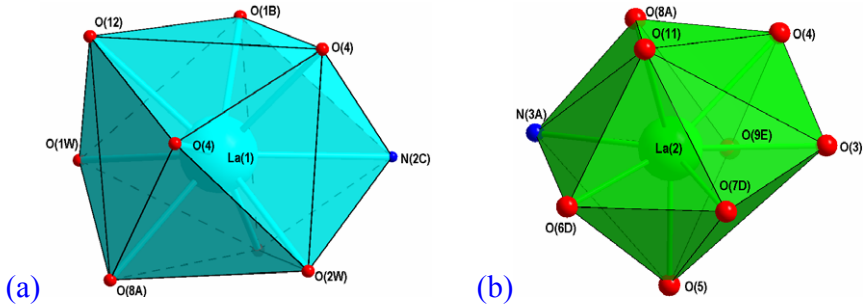

Figure S2. The polyhedral representation of the coordination environments of La(1) (a) and La(2) (b) atoms in **1 ,** (Symmetry code: A: -x, y+1/2, -z+1/2; B: -x+1, -y+2, -z; C: -x+1/2, y+1/2, z; D: x+1/2, y, -z+1/2; E: x-1, y, z).

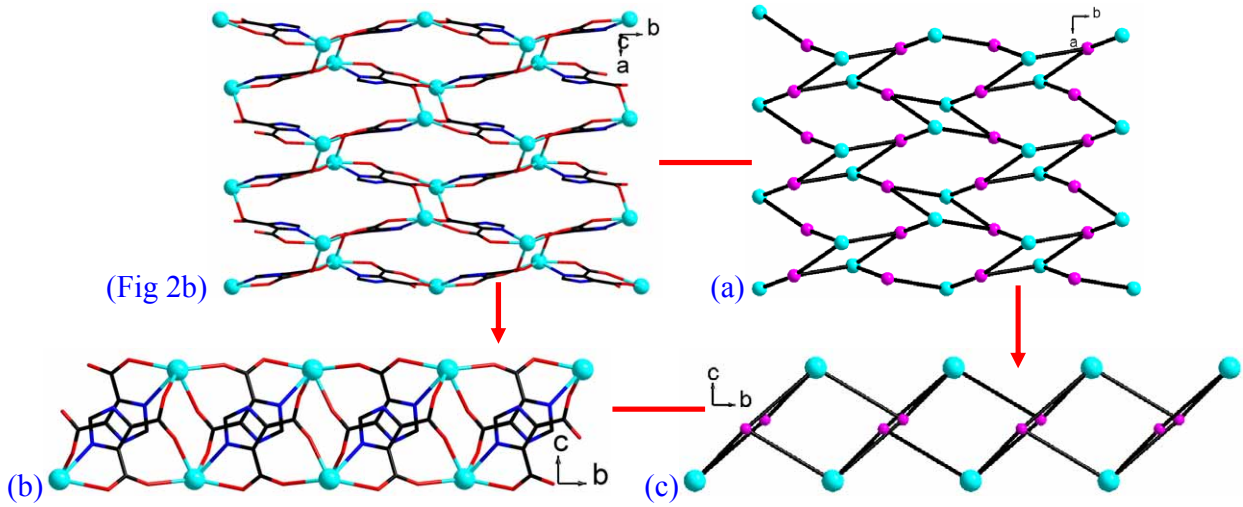

Figure S3. The 2D layer constructed from La(1) and $Himdc_{mode\ 1a}$ viewed along the *c* axis in **1** (Fig 2b); The topology of 2D layer with 4.8^2 net viewed along the *c* axis (a); The 2D layer viewed along the *a* axis (b); The topology of 2D layer with 4.8^2 net viewed along the *a* axis (c). Key: cyan, La(1) ; black, C; blue, N; red, O. The $Himdc_{mode\ 1a}$ units are denoted by purple spheres. La(1) ions and $Himdc_{mode\ 1a}$ ligands function as 3-connected nodes in the net.

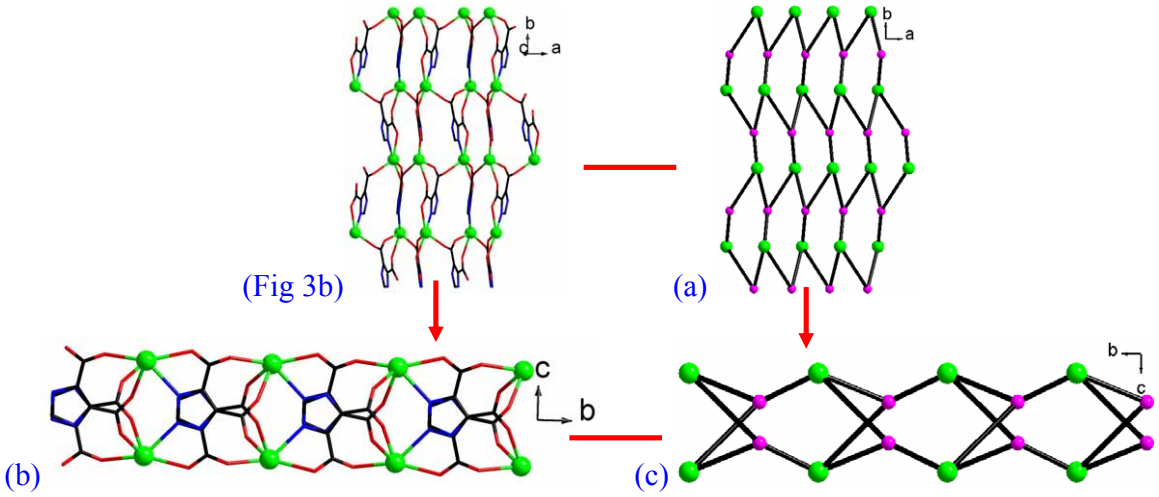

Figure S4. The 2D layer constructed from La(2) and $Himdc_{mode\ 1b}$ viewed along the *c* axis in **1** (Figure 3b); The topology of 2D layer with (6, 3) net viewed along the *c* axis (a); The 2D layer viewed along the *a* axis (b); The topology of 2D layer with (6, 3) net viewed along the *a* axis (c). Key: green, La(2); black, C; blue, N; red, O. The $Himdc_{mode\ 1b}$ units are denoted by purple spheres. La(2) ions and $Himdc_{mode\ 1b}$ units function as 3-connected nodes in the net.

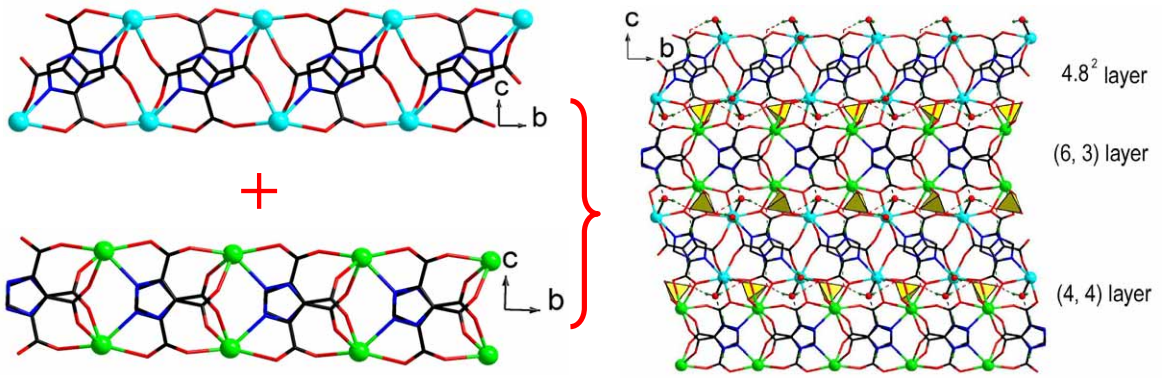

Figure S5. The construction of the packing structure (Right: Figure 4) in combination of {La(1)($Himdc_{mode\ 1a}$)} layer with 4.8^2 net (Left: top) and {La(2)($Himdc_{mode\ 1b}$)} layer (Left: bottom) in **1**.

Figure S6. View of the inorganic $\{La_2O_2\}$ chain running along the [010] direction in **1**: (a) the ball-stick representation; (b) the polyhedral representation. Color: Cyan, La(1); green, La(2); red, O.

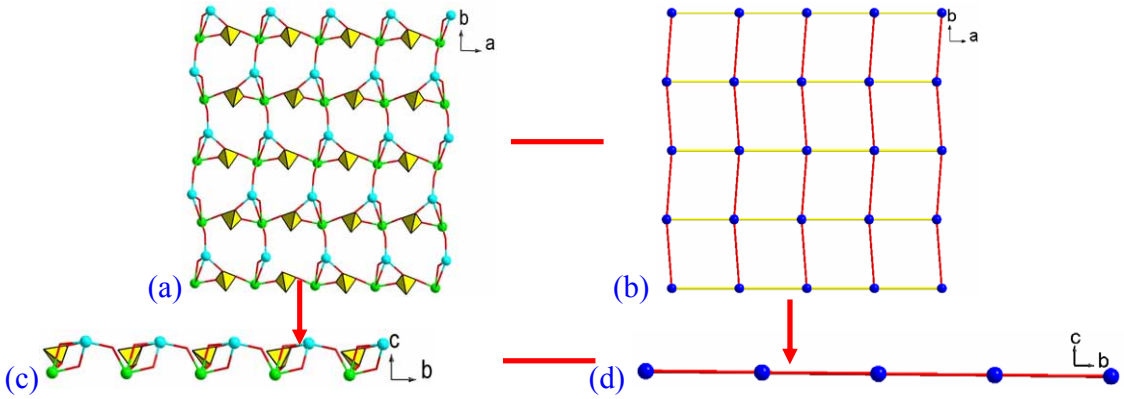

Figure S7. The 2D inorganic layer constructed from inorganic chains and SO_4^{2-} anions viewed along the *c* axis in **1** (a); The topology of 2D layer with (4.4) net viewed along the *c* axis (b); The 2D layer viewed along the *a* axis (c); The topology with (4.4) net viewed along the *a* axis (d). Key: green, La(2); yellow, S; red, O. The La_2O_2 units as 4-conneced nodes are denoted by blue spheres, and the red and yellow lines represent μ_2-O(3) and SO_4^{2-} anions linkers.

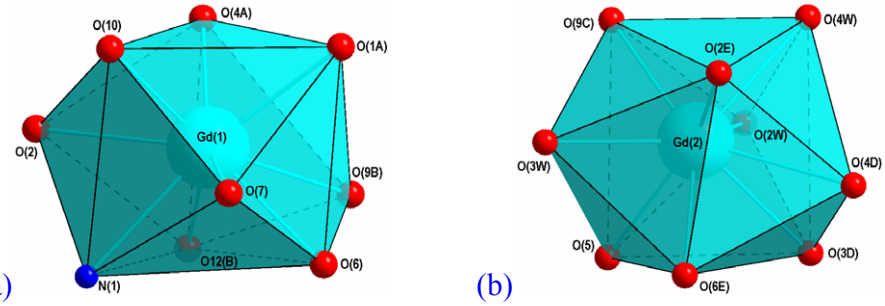

Figure S8. The polyhedral representation of the coordination environments of Gd(1) (a) and Gd(2) (b) atoms in **2.** Atoms having "A", "B" and "C" in their labels are symmetry-generated. Symmetry code: A: -x+2, y-1/2, -z+1/2; B: x, -y+1/2, z-1/2 ; C: -x+1, -y, -z; D: -x+1, -y+1, -z; E: x-1; -y+1/2; z-1/2. Both Gd(1) and Gd(2) ions are nine-coordinated in a tricapped trigonal prism.

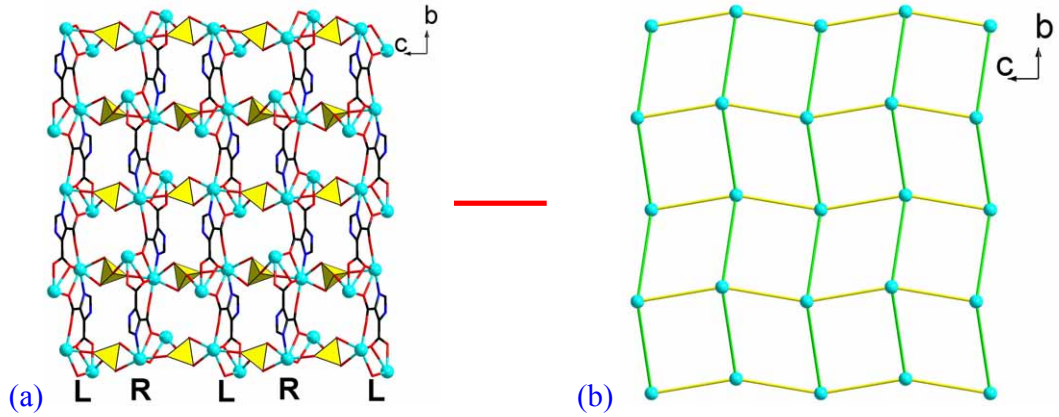

Figure S9. (a) View of the 2D grid layer in **2** along the *a* axis constructed from the alternately connection of left- and right-handed chain by SO_4^{2-} anions. Key: cyan, Gd; black, C; blue, N; red, O; yellow: S. (b) The topology of the 2-D layer with (4, 4)-net. The $[Gd_2O_2]$ units as 4-connected nodes are denoted by cyan spheres, and the yellow and green lines represent $S(1)O_4^{2-}$ anions and Himdc linkers.

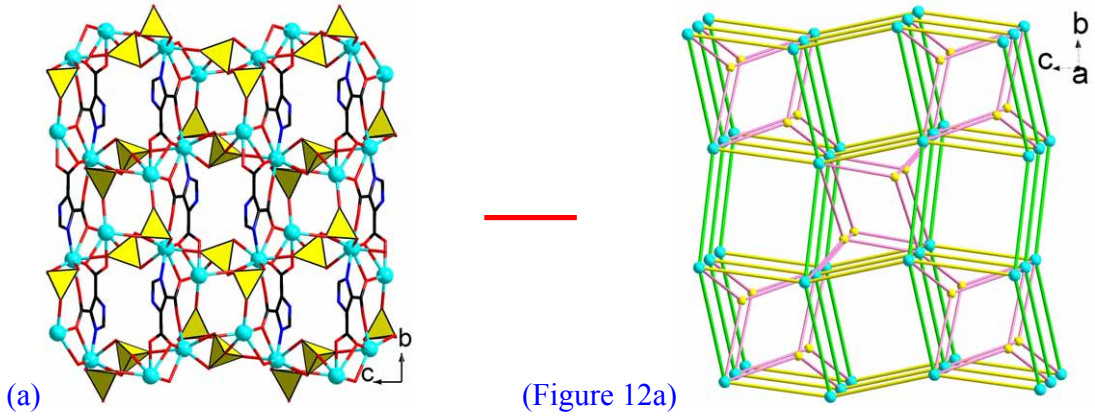

Figure S10. (a) View of 3D framework in **2** along the *a* axis. Key: cyan, Gd; black, C; blue, N; red, O; yellow: S. (Right: Figure 12a) The topology of the 3D framework of **2**, showing the stacking of layers along the [100] direction in an –AAAA- sequence. The $[Gd_2O_2]$ units as 4-connected nodes are denoted by cyan spheres, and the yellow and green lines represent $S(1)O_4^{2-}$ anions and Himdc linkers.

This journal is © The Royal Society of Chemistry 2007

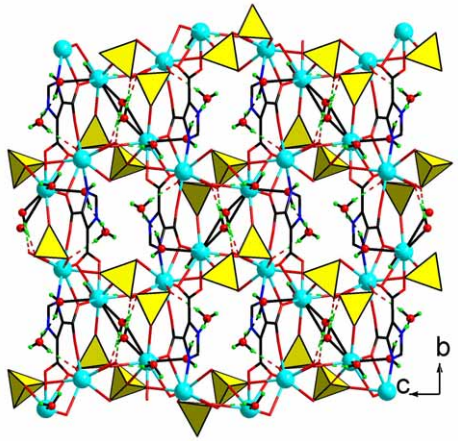

Figure S11. The H-bonding network in the structure of **2**. Key: cyan, Gd; black, C; blue, N; red, O; yellow: S.

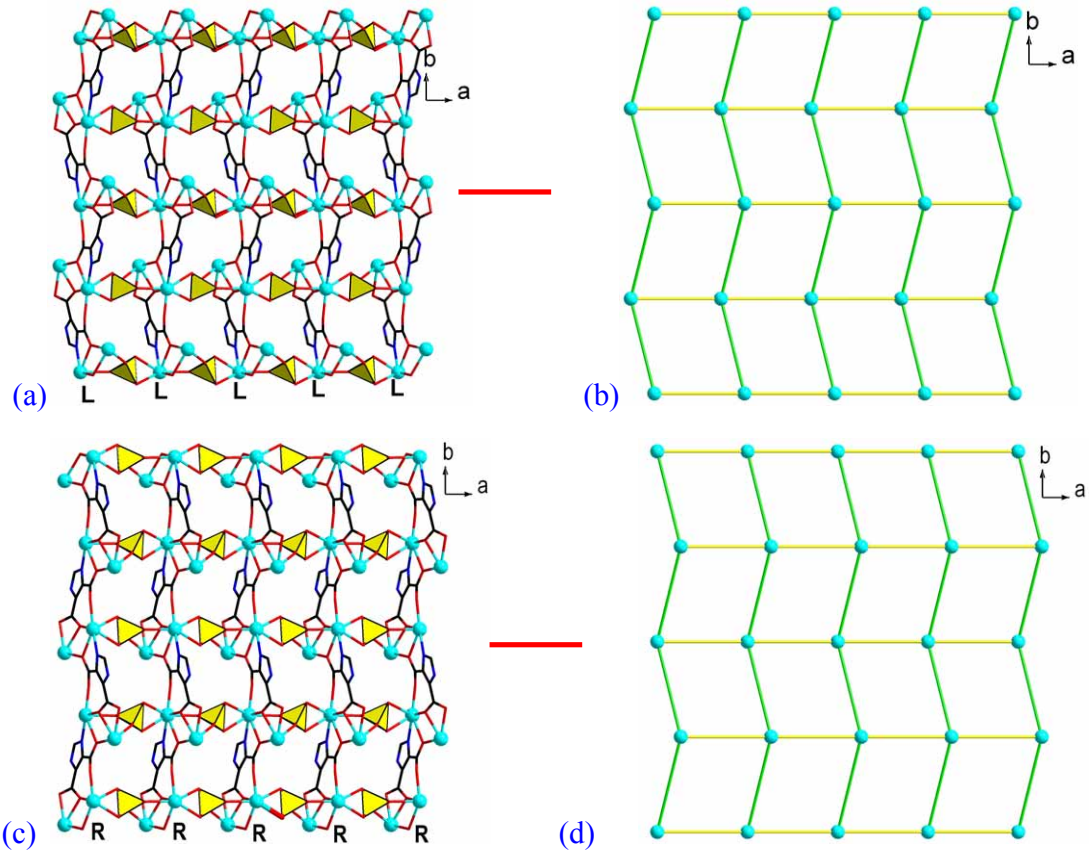

Figure S12. (a) View of the 2D grid layer in **3a** along the *c* axis made of single left-handed chains and SO_4^{2-} anions. (b) The topology of the 2D layer made of single left-handed chains and SO_4^{2-} anions with (4, 4)-net. (c) View of the 2D grid layer in **3a** made of single right-handed chains and SO_4^{2-} anions. (d) The topology of the 2D layer made of single right-handed chains and SO_4^{2-} anions. Key: cyan, Gd; black, C; blue, N; red, O; yellow: S. The $[Gd_2O_2]$ units as 4-connected nodes are denoted by cyan spheres, and the yellow and green lines represent $S(1)O_4^{2-}$ anions and Himdc linkers.

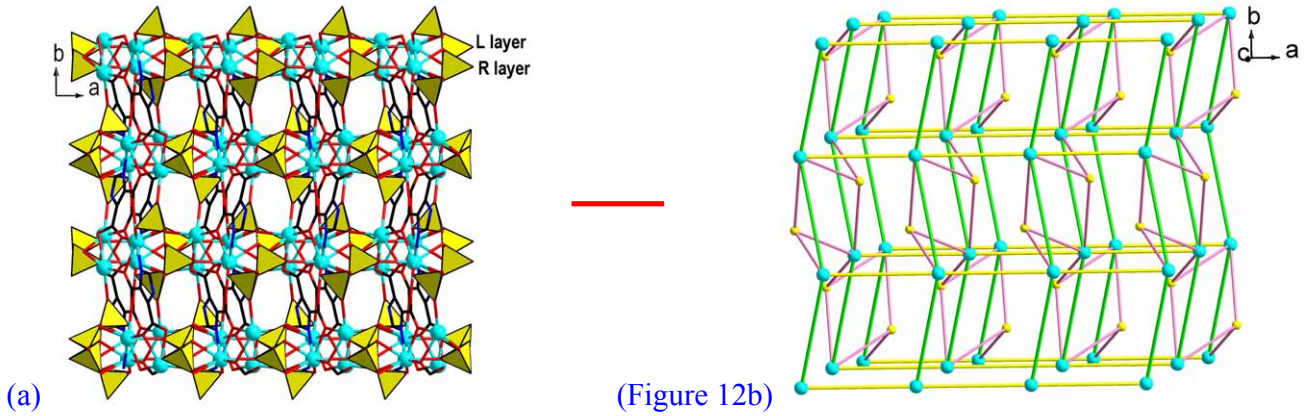

Figure S13. (a) View of 3-D framework in **3a** along the *c* axis. (Right: Figure 12b) The topology of the 3D framework of **3a**, showing the alternately connection of left- and right-handed layers by SO_4^{2-} anions. Key: cyan, Gd; black, C; blue, N; red, O; yellow: S. The $[Gd_2O_2]$ units as 4-connected nodes are denoted by cyan spheres, and the yellow and green lines represent $S(1)O_4^{2-}$ anions and Himdc linkers.

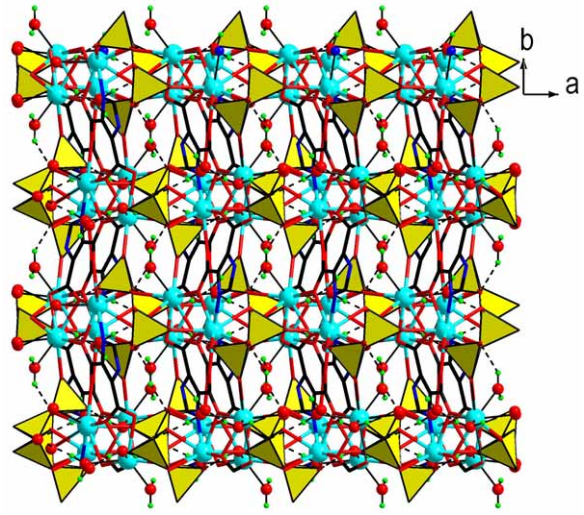

Figure S14. The H-bonding network in the structure of **3a**. Key: cyan, Gd; black, C; blue, N; red, O; yellow: S.

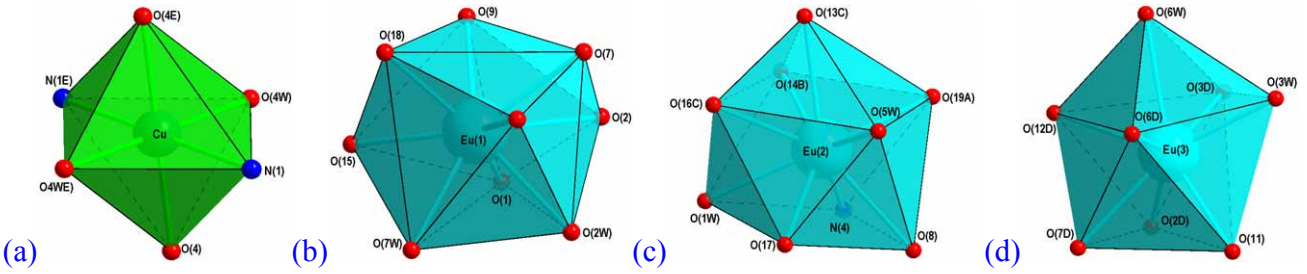

Figure S15. The polyhedral representation of the coordination environments of Cu (a), Eu(1) (b), Eu(2) (c) and Eu(3) (d) atoms in **4.**

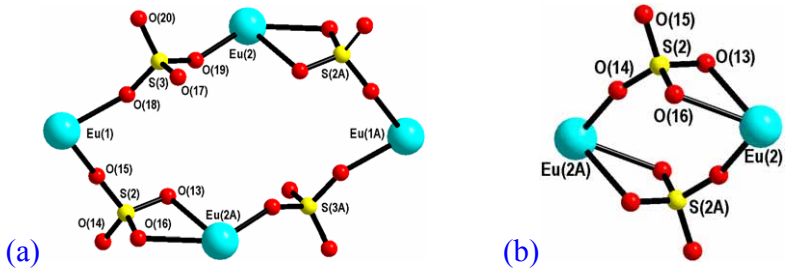

Figure S16. Ball-stick representation of the 8-membered ring (a) and 4-membered ring (b) in **4**.

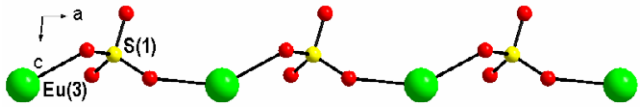

Figure S17. 1D $\{EuSO_4\}$ chain constructed from $Eu(3)^{3+}$ and $S(1)O_4^{2-}$ anions running along the *a* axis in **4**.

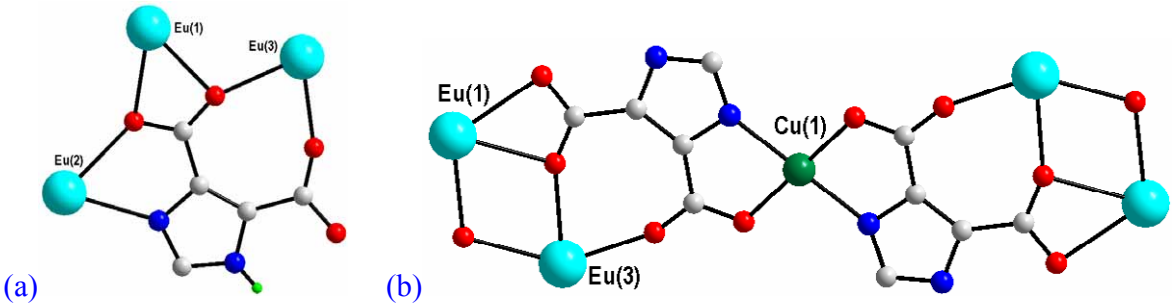

Figure S18. Coordination modes of Himdc in **4**: (a) behaving as an ancillary ligand chelated with the Eu atoms to decorate the 2D tubular layer; (b) Coordinated to Cu atoms to form $[Cu(Himdc)_2]$ complexes, which support the adjacent tubular layers to generate the 3D open framework . Key: cyan, Eu; black, C; blue, N; red, O; green: Cu.

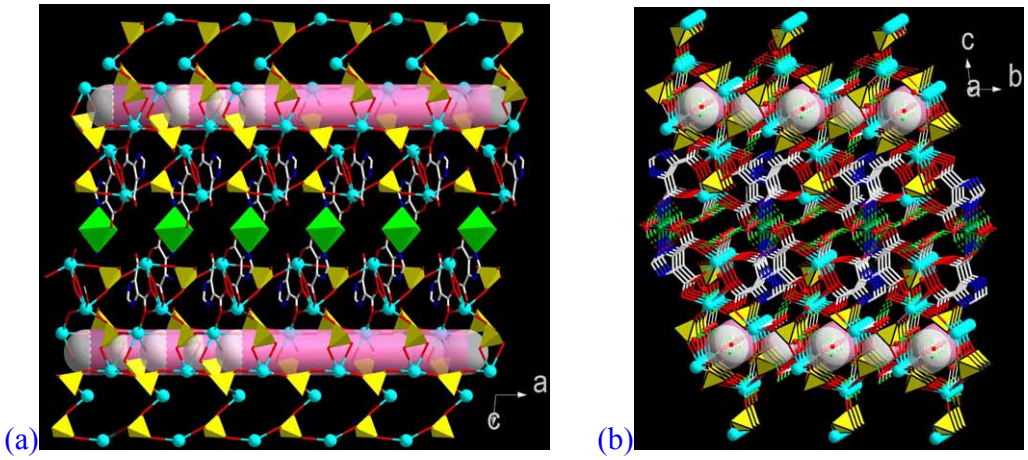

Figure S19. (a) The stacking of **4** viewed along the *b* axis, showing the 1D channels. (b) The 3D framework of **4** viewed along the approximate the *a* axis, showing the H-bond network. Key: cyan, Eu; black, C; blue, N; red, O; yellow: S; green, Cu.

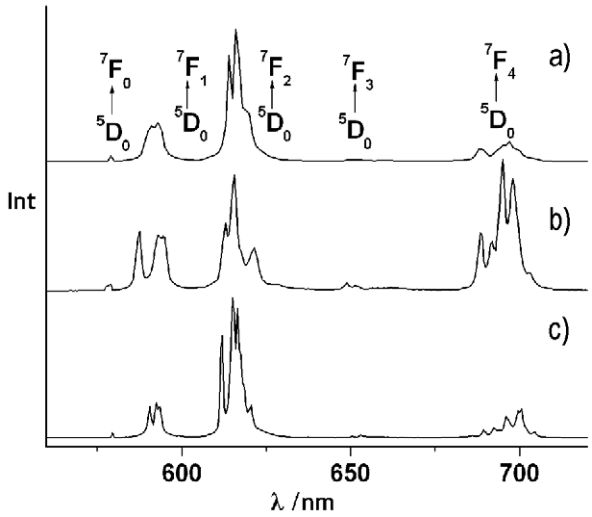

Figure S20. Emission spectra of **3b**(a), **4**(b) and **5a** (c) in solid state at room temperature (all excitation at 394 nm).

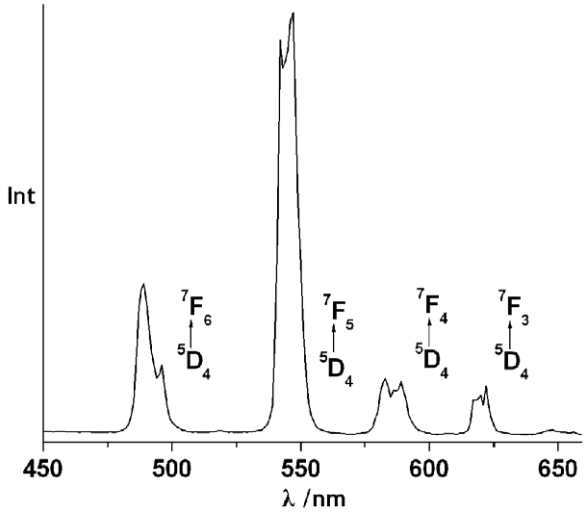

Figure S21. Emission spectra of **5c** in solid state at room temperature (excitation at 344nm).

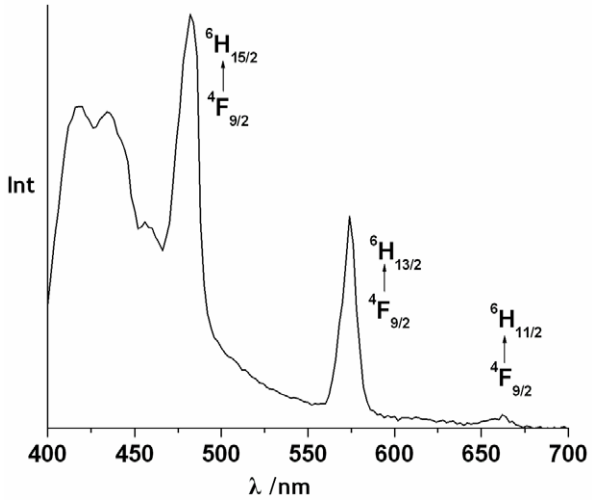

Figure S22. Emission spectra of **5d** in solid state at room temperature (excitation at 352nm).

Luminescent Properties. Complex **3b** yields intense red luminescence (Figure S20a) and exhibits the characteristic transition of $^5D_0 \rightarrow {}^7F_J$ (J = 0–4) of the Eu^{3+} ion with a decay lifetime of 209.4 μs for $^5D_0 \rightarrow {}^7F_2$. It can be seen that the intensity ratio of $^5D_0 \rightarrow {}^7F_2$ /$^5D_0 \rightarrow {}^7F_1$ is 3.4 which indicates that the Eu^{3+} ions are not in an inversion center, which further confirms by the appearance of the symmetric forbidden emission $^5D_0 \rightarrow {}^7F_0$ at 579 nm. This is in agreement with the result of the single crystal X-ray analysis. It is noticed that the bands originated from the $^5D_0 \rightarrow {}^7F_3$ transition is of low intensity and may be taken as forbidden. The luminescent properties of lanthanide complexes are very dependant on the local environments around the lanthanide centres, such as the coordinating ligand, symmetry of the ligand filed, and related coordination environments. When **4** was excited at 394 nm, the characteristic red emission spectra were recorded at 580, 594, 615, 649, and 695 nm, which are ascribed to the transition of $^5D_0 \rightarrow {}^7F_J$ (J=0–4), respectively with a decay lifetime of 337.0 μs for $^5D_0 \rightarrow {}^7F_2$ (Figure S20b). The intensity of the $^5D_0 \rightarrow {}^7F_0$ transition is relative weak and the emission band is not symmetrical, which suggests that the Eu^{3+} are not in an inversion centers. The splitting of the two Stark components of the $^7F_1$ multiplet indicates the presence of more than one chemically different Eu^{3+} ion sites. The intensities of $^5D_0 \rightarrow {}^7F_{2,4,6}$ transitions are strongly dependent on the odd-parity components of the crystal field. Different from **3b**, the $^5D_0 \rightarrow {}^7F_4$ is the strongest one in the five transitions in **4**, which is very interesting and rarely observed in Eu complexes. The result shows that Eu^{3+} ions have lower symmetric coordination environment in **4**. This is in agreement with the result of the single crystal X-ray analysis. In general, the luminescent intensity of the Ln^{3+} depends on the efficiency of the energy transfer. The difference of the emission spectra of **3b** and **4** may result from the incorporation of Cu^{2+} ions in **4**, which make the energy transfer process of $^5D_0 \rightarrow {}^7F_4$ more effective. **5a** yields intense red luminescence (Figure S20c) and exhibits the characteristic transition of $^5D_0 \rightarrow {}^7F_J$ (J=0–4) of the Eu^{3+} ion with a decay lifetime of 256 μs for $^5D_0 \rightarrow {}^7F_3$. The $^5D_0 \rightarrow {}^7F_0$ transition observed as a weak peak at 579 nm reveals the presence of the Eu^{3+} site with low symmetry. The $^5D_0 \rightarrow {}^7F_2$ transition is clearly stronger than the $^5D_0 \rightarrow {}^7F_1$, the intensity ratio of 3.9 for $I(^5D_0 \rightarrow {}^7F_2)/I(^5D_0 \rightarrow {}^7F_1)$, which indicates the absence of inversion center at Eu^{3+} site. This is in agreement with the result of the single crystal X-ray analysis.

Complex **5c** is green-luminescent (Figure S21) in solid state with a typical Tb^{3+} emission at 489, 547, 583 and 622 nm, corresponding to the characteristic emission $^5D_4 \rightarrow {}^7F_J$ (J = 6-3) transitions of Tb^{3+} ion. The spectrum is dominated by the $^5D_4 \rightarrow {}^7F_5$ transition, at 547 nm, which gives an intense green luminescence output for the solid sample. The lifetime of complex **5c** for $^5D_4 \rightarrow {}^7F_5$ is 0.49 ms. No emission bands from the ligands or LMCT are observed in complexes **5a** and **5c**, indicating that the Himc ligands transfer the excitation energy efficiently to the Eu^{3+} and Tb^{3+} centers. Two emission groups for **5d** in the range of 400-450 and 450-680 nm are shown in Figure S22. The emission at 482, 574 and 662 nm (decay lifetime = 0.946 μs for the transition of $^4F_{9/2} \rightarrow {}^6H_{15/2}$) is attribute to the characteristic emission of $^4F_{9/2} \rightarrow {}^6H_J$ (J = 15/2, 13/2 and 11/2) transitions of Dy^{3+} ion. It is obvious that the intensity of the blue emission corresponding to $^4F_{9/2} \rightarrow {}^6H_{15/2}$ transition is much stronger than that of the yellow one, which indicates that H_2imc acts as a better sensitizer to the blue Dy^{3+} emission, unlike the previously reported imdc-based Dy^{3+} complex which gives predominantly yellow luminescence. The large broad blue-shift band ranging 400 to 450 nm would be assigned to the emission of ligand-to-metal charge transfer (LMCT). The intensity of the metal centered transitions is strong, relatively

to that of the broad LMCT band, which actually implies that direct metal excitation is comparable with the sensitized process, as the extinction coefficients of the metal emission are much lower than that of the ligands.

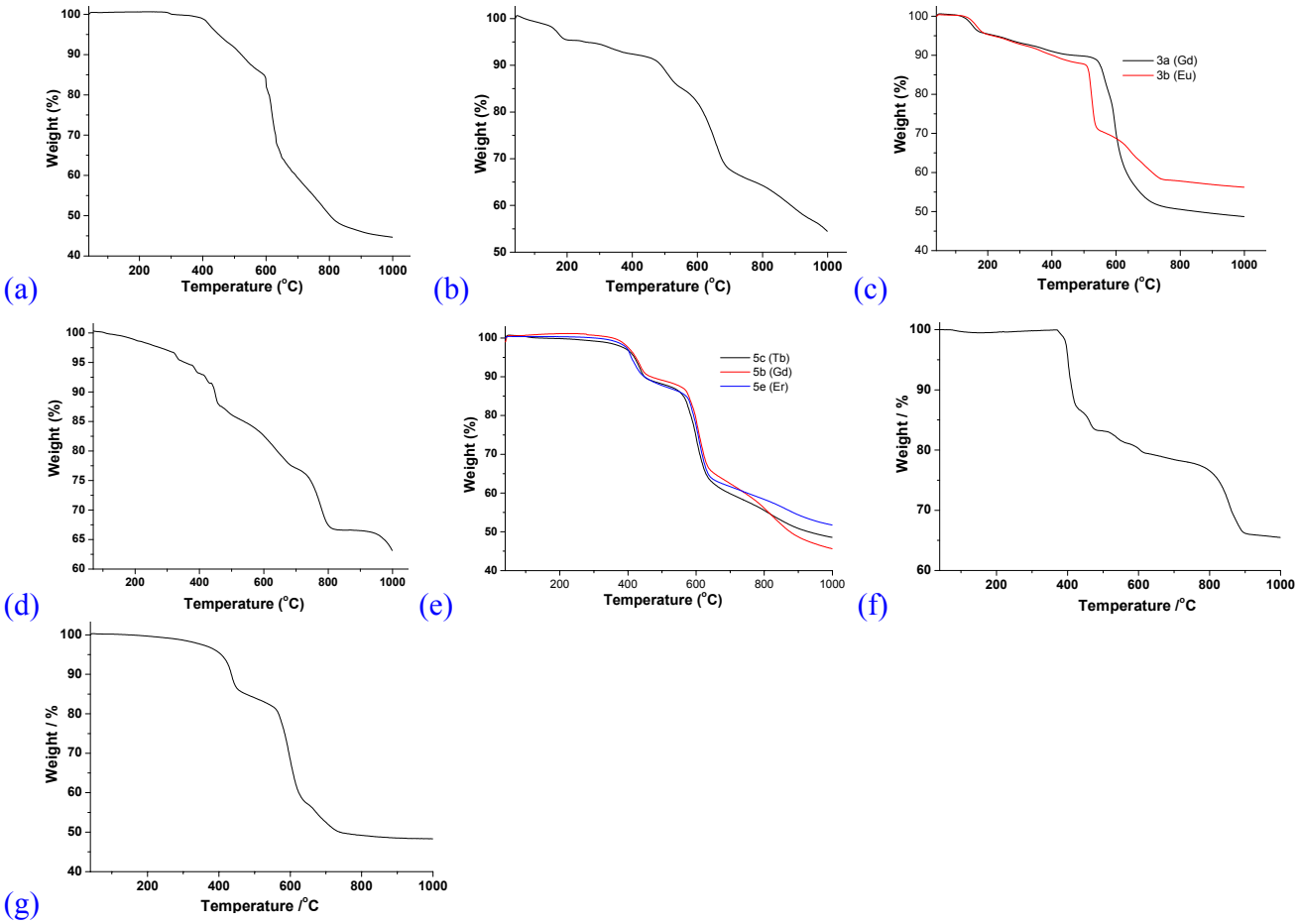

Figure S23. TG curves for **1** (a), **2** (b), **3a/3b** (c), **4** (d), **5b/5c/5e** (e), **5a** (f) and **5d** (g) under air atmosphere (10 °C/min).

Thermogravimetric analyses of these materials were performed to investigate their thermal stability. In the TG curve of **1**, there is only one weight loss of 54.8% in the temperature rang 300-950 ºC, corresponding to the successive release of two coordinated waters, decomposition of two Himdc and departure of one SO_4^{2-} anion as SO_3. Assuming that the residue corresponds to La_2O_3, the observed total weight loss (45.2%) is in agreement with the calculated value (45.4%) (Figure S23a).

The TG curve of **2** shows that the initial weight loss between 70 and 200 ºC corresponds to the release of one lattice water molecule and one coordinated water molecule per formula unit (calcd/found: 4.9/4.6%). Then, further decomposition of **2** begins above 200 ºC, and the residues at 1000 ºC might be $Gd_2O(SO_4)_2$[1] (obsed/calcd: 54.5/54.9%), a mixture containing 1/2 $Gd_2O_2(SO_4)$ and 1/2 $Gd_2(SO_4)_3$ (Figure S23b).

TGA of **3a** shows three regions of weight loss. The first, a mass loss of 4.6% from 100 to 200 ºC, corresponds to the loss of one lattice water molecule and one coordinated water molecule (calcd 4.9%). Then, the weight loss between 200 and 450 ºC is assigned to the removal of the remaining two coordinated water molecules (calcd/found: 4.9/5.3%). Above this temperature, the complex begins to decompose, and at 900 ºC the residue is Gd_2O_3 (calcd/found: 49.5/ 49.5%)(Figure S23c).

As shown in Figure S23c, compound **3b** also shows three regions of weight loss. The first, a mass loss of 4.7% for **3b** from 100 to 200ºC, corresponds to the loss of one lattice water molecule and one coordinated water molecules (calcd 5.0% for **3b**). Then, the weight loss between 200 and 400 ºC for **3b** is assigned to the removal of the remaining two

coordinated water molecules (calcd/found: 5.0%/5.2% for **3b**). Above the temperature, the compounds begin to decompose, and at 740ºC the residue of **3b** is $Eu_2O_2(SO_4)$ (calcd/found: 59.8/58.4%).

The TG plot of **4** shows that only one weight loss is observed between 100 and 830 ºC, which is assigned to the successive removal of one coordinated water and one Himdc. The residues at 830 ºC have a composition of $[Eu_6CuO_4(SO_4)_6]$ corresponding to $2Eu_2(SO_4)_3 \cdot Eu_2O_3 \cdot CuO$ (calcd/found: 66.8/66.6%). Then the residues keep stable and at 930 ºC begin to decompose (Figure S23d).

The TG curve of **5a** also displays two continuous weight loss stages in the range of 350-1000 ºC, corresponding to the successive release of one coordination water molecule and one ligand per formula unit (obsed/calcd: 33.8/32.1%). The 66.2% white residue is close to the weight of $Eu_2O(SO_4)_2$ (calcd: 67.9%). The $Eu_2O(SO_4)_2$ might be a mixture containing 1/2 $Eu_2(SO_4)_3$ and 1/2 $Eu_2O_2(SO_4)$(Figure S23f).

As shown Figure S23e, the TG curves of **5b** and **5e** show similar thermal behavior and undergo one weight loss, corresponding to the release of one coordination water molecule and one ligand, and/or the departure of one sulfate as SO_3 per formula unit. The residue had a composition of Gd_2O_3 for **5b** at 930ºC (calcd/found: 47.4/47.8%); $Er_2O_2SO_4$ for **5e** at 800 ºC (calcd/found: 58.9/58.3%).

The TG curve of **5c** displays the weight loss of 51.4 %(calcd 51.3%) from 140-1000 ºC corresponds to the release of one coordination water molecule and one ligand, and/or the departure of one sulfate as SO_3 per formula unit. The 48.6% white residue might be Tb_4O_7 (calcd: 48.7%) per formula unit (Figure S23e).

In the TG curve of **5d** shows two continuous weight loss stages in the range of 150-900 ºC, corresponding to the successive release of one coordination water molecule, one ligand and/or the departure of one sulfate as SO_3 per formula unit (obsed/calcd: 51.7/51.9%). The 48.3% white residue might be Dy_2O_3 (calcd: 48.1%)(Figure S23g).

1. T. Bataille and D. Louër, *J. Solid State Chem.*, 2004, **177**, 1235.

Table S1. Crystal data and Structure Refinements for Compounds **3a-5e**

	3b	**5b**	**5c**	**5d**	**5e**
Formula	$C_5H_{10}Eu_2N_2O_{16}S_2$	$C_4H_5GdN_2O_7S$	$C_4H_5N_2O_7STb$	$C_4H_5DyN_2O_7S$	$C_4H_5ErN_2O_7S$
Fw	722.21	382.41	384.08	387.66	392.42
Crystal system	Monoclinic	Monoclinic	Monoclinic	Monoclinic	Monoclinic
Space group	P21/c	P21/c	P21/c	P21/c	P21/c
a/Å	6.602 (1)	11.207(1)	11.181(1)	11.157(3)	11.147(1)
b/Å	13.324(1)	6.525 (1)	6.498(1)	6.479(2)	6.447(1)
c/Å	18.880(1)	12.182(1)	12.132(1)	12.087(3)	12.039(1)
β/°	106.62(1)	107.91(1)	107.82(1)	107.82(1)	107.77 (1)
V/Å	1591.4(2)	847.7(1)	839.1 (1)	831.8(4)	823.9(1)
Z	4	4	4	4	4
Dc/g cm^{-3}	3.014	2.996	3.040	3.096	3.164
μ/mm^{-1}	8.166	8.091	8.698	9.256	10.462
F(000)	1360	716	720	724	732

This journal is © The Royal Society of Chemistry 2007

S(F2)	1.110	1.146	1.113	1.014	1.208
R1,(I>2σ (I))	0.0288	0.0347	0.0269	0.0204	0.0314
wR2 (I>2σ (I))	0.0735	0.0869	0.0667	0.0441	0.0777

Table S2. Geometrical Parameters of Hydrogen Bonds for **type I – type V.**

D-H	d(D-H)	d(H..A)	<DHA	d(D..A)	A	
1						
N1-H1	0.87	1.94	163	2.791	O10	[x-1/2, -y+3/2, -z]
N4-H4	0.86	2.09	167	2.934	O1W	[-x+1/2, y-1/2, z]
O1W-H12	0.80	1.89	161	2.659	O10	[-x+3/2, y+1/2, z]
O1W-H11	0.75	2.42	111	2.770	O12	
O2W-H21	0.71	2.40	137	2.952	O12	[x-1, y, z]
O2W-H22	0.64	2.18	168	2.802	O1	[-x, -y+2, -z]
2						
N2-H1	0.95	2.03	160	2.947	O1W	[-x+1,-y+1,-z]
O1W-H11	0.77	2.00	169	2.766	O10	[x,-y+1/2,z-1/2]
O2W-H21	0.77	2.04	153	2.749	O11	
O3W-H31	0.77	2.05	149	2.737	O8	[x-1,-y+1/2,z-1/2]
O3W-H32	0.71	2.15	152	2.797	O11	[-x+1,-y,-z]
O4W-H42	0.93	1.86	163	2.760	O1W	[-x+1,y-1/2,-z-1/2]
3a						
N2-H2A	0.86	2.06	165	2.891	O1W	[-x,-y,-z-1]
O2W-H21	0.90	2.07	164	2.944	O6	[x-1,y,z]
O3W-H31	0.90	1.90	161	2.764	O11	[x,-y-1/2,z+1/2]
O3W-H32	0.89	1.86	157	2.701	O10	[x-1,-y-1/2,z+1/2]
O4W-H41	0.91	2.22	120	2.796	O11	[-x,y+1/2,-z-1/2]
3b						
N2-H2A	0.86	2.07	164	2.901	O1W	[-x,-y,-z-1]
O2W-H21	0.89	2.09	162	2.945	O6	[x-1,y,z]
O3W-H31	0.90	1.90	164	2.772	O11	[x,-y-1/2,z+1/2]
O3W-H32	0.85	1.90	156	2.704	O10	[x-1,-y-1/2,z+1/2]
O4W-H41	0.91	2.24	120	2.805	O11	[-x, y+1/2,-z-1/2]
4						
N2-H2A	0.86	1.96	168	2.811	O20	[x,y+1,z]
N3-H3A	0.86	2.06	162	2.889	O10	[x-1,y-1,z]
O1W-H11	0.85	2.29	112	2.724	O16	[-x+2,-y,-z+1]
O1W-H12	0.86	2.01	146	2.772	O1	[x,y-1,z]
O2W-H21	0.89	2.13	141	2.869	O9	[x-1,y,z]
O3W-H31	0.93	2.22	133	2.931	O3	[x+1,y,z]
O3W-H31	0.93	2.22	137	2.971	O6W	
O4W-H41	0.91	1.76	167	2.656	O5	[x+1,y+1,z]
O4W-H42	0.91	2.00	153	2.845	O5	[-x+2,-y,-z]
O5W-H51	0.84	2.03	154	2.809	O7W	
O6W-H61	0.84	1.94	159	2.746	O4W	[-x+3,-y,-z]
O6W-H62	0.83	2.25	120	2.752	O12	[x+1,y,z]
O7W-H72	0.89	1.92	150	2.721	O16	
O7W-H71	0.89	1.95	155	2.782	O13	[x-1,y,z]
5a						
O1W-H11	0.84	2.06	160	2.865	O4	[-x, y-1/2, -z+3/2
O1W-H12	0.83	1.95	174	2.773	O2	[-x, -y, -z+1]
N1-H1B	0.86	2.34	127	2.933	O4	[x+1, y, z]
5b						
O1W-H11	0.85	2.05	160	2.860	O4	[-x,y-1/2,-z+3/2]
O1W-H12	0.83	1.97	173	2.794	O2	[-x,-y,-z+1]
N1-H1B	0.86	2.33	128	2.942	O4	[x+1,y,z]
5c						
O1W-H11	0.84	2.06	160	2.862	O4	[-x,y-1/2,-z+3/2]
O1W-H12	0.83	1.95	173	2.778	O2	[-x,-y,-z+1]
N1-H1B	0.86	2.34	127	2.939	O4	[x+1,y,z]
5d						
O1W-H11	0.85	2.06	160	2.865	O4	[-x, y-1/2, -z+3/2
O1W-H12	0.83	1.97	173	2.795	O2	[-x, -y, -z+1]
N1-H1B	0.86	2.32	128	2.921	O4	[x+1, y, z]
5e						

This journal is © The Royal Society of Chemistry 2007

O1W-H11	0.84	2.07	160	2.871	O4	[-x,y-1/2,-z+3/2]
O1W-H12	0.83	1.93	174	2.754	O2	[-x,-y,-z+1]
N1-H1B	0.86	2.38	125	2.955	O4	[x+1,y,z]